Obrabotka metallov (tekhnologiya, oborudovanie, instrumenty) = Metal Working and Material Science. 2025 vol. 27 no. 4 pp. 116–130
ISSN: 1994-6309 (print) / 2541-819X (online)
DOI: 10.17212/1994-6309-2025-27.4-116-130

NSTU NETI

Obrabotka metallov - Metal Working and Material Science

Journal homepage: http://journals.nstu.ru/obrabotka_metallov

Optimal milling parameters of 0.12 C-18 Cr-10Ni-Ti stainless steel fabricated by electron beam additive manufacturing

Mengxu Qi [1, a], ***Sergey Panin*** [2, b, *], ***Dmitry Stepanov*** [2, c], ***Mikhail Burkov*** [2, d], ***Qingrong Zhang*** [1, e]

[1] National Research Tomsk Polytechnic University, 30 Lenin Avenue, Tomsk, 634050, Russian Federation
[2] Institute of Strength Physics and Materials Sciences SB RAS, 2/4 per. Academicheskii, Tomsk, 634055, Russian Federation

[a] https://orcid.org/0000-0003-3738-0193, mensyuy1@tpu.ru; [b] https://orcid.org/0000-0001-7623-7360, svp@ispms.ru;
[c] https://orcid.org/0000-0003-2558-7613, sdu@ispms.ru; [d] https://orcid.org/0000-0002-3337-6579, burkovispms@mail.ru;
[e] https://orcid.org/0009-0002-7820-1227, cinzhun1@tpu.ru

ARTICLE INFO

Article history:
Received: 08 September 2025
Revised: 01 October 2025
Accepted: 29 October 2025
Available online: 15 December 2025

Keywords:
Additive manufacturing
AISI 321
Electron beam additive manufacturing
Milling
Multiple regression method
Feed-Forward Neural Network

Funding
The study was financially supported by the Russian Federation via Ministry of Science and Higher Education of the Russian Federation (Agreement No. 075-15-2023-456).

Acknowledgements
Research were conducted at core facility "Structure, mechanical and physical properties of materials" NSTU. The authors thank Yu.V. Kushnarev for assistance in fabricating *0.12C-18Cr-10Ni-Ti* steel samples at the experimental facility of ISPMS SB RAS.

ABSTRACT

Introduction. Unlike traditional manufacturing processes, additive manufacturing (*AM*) offers improved efficiency while being environmentally friendly. A significant limitation hindering the adoption of wire-based electron beam additive manufacturing (*EBAM*) technology is the relatively low quality and high surface roughness of 3D-printed parts. **The purpose of this study** is to establish the optimal values of milling process parameters (rotational speed, feed rate, and milling width) based on the simultaneous evaluation of the surface roughness of the machined surface and the material removal rate. **Methods and materials.** This study investigated specimens fabricated using *EBAM* technology. Uniaxial tensile tests were conducted on an electromechanical testing machine. Cutting forces were determined with a *Kistler 9257B* dynamometer. Milling studies of *EBAM* 321 steel workpieces were performed on a semi-industrial *CNC* milling machine. **Results and discussion.** It was shown that in order to increase the material removal rate and reduce the cutting force on a milling machine without the use of coolant, it is recommended to increase the milling speed, but not to increase the feed rate. To investigate the relationship between material removal rate and surface roughness relative to milling parameters on a semi-industrial machine (with an average stiffness of the portal frame), multiple linear regression models and nonlinear models based on feedforward neural networks were employed. It was demonstrated that linear regression models are sufficient for predicting optimal milling parameters. However, it should be noted that the study was conducted within a narrow range of gentle machining conditions, with short processing times and without accounting for tool wear. Under these constraints, the optimal milling parameters for *EBAM 321* steel were predicted as follows: spindle speed of 4,500 rpm, feed rate $\boldsymbol{S}$ = 404 mm/min, and cutting depth $\boldsymbol{B}$ = 0.43 mm, resulting in a predicted surface roughness ($\boldsymbol{Ra}$) of 0.648 μm and a material removal rate of 695 mm³/min.

For citation: Qi M., Panin S.V, Stepanov D.Y., Burkov M.V., Zhang Q. Optimal milling parameters of 0.12 C-18 Cr-*10Ni-Ti* stainless steel fabricated by electron beam additive manufacturing. *Obrabotka metallov (tekhnologiya, oborudovanie, instrumenty) = Metal Working and Material Science*, 2025, vol. 27, no. 4, pp. 116–130. DOI: 10.17212/1994-6309-2025-27.4-116-130. (In Russian).

*** Corresponding author**
Panin Sergey V., D.Sc. (Engineering), Professor
Institute of Strength Physics and Materials Sciences SB RAS,
2/4 per. Academicheskii,
634055, Tomsk, Russian Federation
Tel.: +7 3822 286-904, **e-mail:** svp@ispms.ru

Introduction

Traditionally, stainless steels are classified into five categories: (*I*) austenitic, (*II*) ferritic, *III*) martensitic, (*IV*) duplex, and (*V*) precipitation-hardened. Among them, the austenitic steels are the most widely used in terms of fabricated metal products [1]. *AISI 321* steel possesses excellent resistance to intercrystalline corrosion and maintains stable functional properties at elevated temperatures. Therefore, it is often used under severe conditions, such as high pressures, radiation exposure, and corrosive environments [2–3].

Unlike traditional subtractive manufacturing technologies, additive manufacturing (*AM*) offers several advantages: reduced production time, increased material utilization rate, and the ability to create complex internal structures within components. When applied to metallic materials, *AM* includes various methods: Selective Laser Melting (*SLM*), Electron Beam Selective Melting (*EBSM*), Wire Laser AM (*WLAM*), Wire Arc AM (*WAAM*), and Electron Beam Wire-Feed AM (*EBWAM*) [3–16]. Compared with *WLAM* and *WAAM*, electron beam wire-feed *AM* (*EBWAM*) is characterized by a higher production rate (up to 12 kg/h [7]), as well as reduced atmospheric contamination [8] and spatter of molten material [9, 10].

In recent years, additive manufacturing (*AM*) has rapidly expanded its application scope due to a range of advantages. This production method enables the fabrication of complex-shaped parts with high precision using various materials, from plastics to metals, while significantly reducing time and costs compared to traditional manufacturing technologies [1–4]. Depending on the requirements for the final product, different *AM* technologies are employed. Active development of *AM* leads to a reduction in product cost. It makes rapid production possible for parts and workpieces with not only complex geometries but also simpler shapes made of expensive materials [5–6]. Flanges made of heat-resistant materials are an example of such parts. When using *AM*, there is no need to create holes through drilling; moreover, the volume of material removed through subtractive processing is reduced. This economically justifies the application of *AM*. The use of *AM* for manufacturing flanges allows them to be tailored to specific sizes, resulting in even greater time and cost savings compared to the production of similar parts from wrought stock [7–9].

A specific limitation hindering the adoption of wire-based additive manufacturing technology is the low dimensional (shape) accuracy and high surface roughness of as-built parts [14]. Powder-based additive manufacturing technologies (specifically SLM) enable the production of parts with high dimensional accuracy and low surface roughness. However, even they cannot match the surface roughness achieved by finish turning and/or finish milling [16], necessitating post-process machining.

On the other hand, compared to powder-based processes, the wire-based *AM* methods, particularly the *EBWAM* method, offer higher production rates and are better suited for manufacturing large-sized products [6–10]. Consequently, parts produced by wire-based *AM* inevitably require subsequent machining. Thus, the development of hybrid technologies that combine additive and subtractive manufacturing processes is receiving significant attention in scientific and technical literature [16].

Additive manufacturing also offers advantages in customization, prototyping, and the fabrication of complex geometries; however, it is generally unsuitable for large-scale mass production, which often requires the use of expensive, dedicated multi-axis machining equipment. In contrast, semi-industrial (light-duty, universal) milling machines are cheaper and more flexible to reconfigure compared to traditional industrial equipment. They are typically used for small-batch, custom production or can be effective during the stage of optimizing process parameters for post-additive machining.

Given the demand for wire-based *AM* technologies, the use of semi-industrial (light-duty, universal) *CNC* milling machines within a unified technological cycle alongside *3D*-printing systems appears promising. This approach would not only allow for the adaptive selection of machining parameters for the printed workpiece, primarily based on criteria for improving accuracy and reducing surface roughness, but also enable the establishment of a correlation between the process parameters of *AM* and the resulting machinability. The latter could also minimize the scope of required metallurgical investigations.

In this context, it is relevant to study the machinability of wire-feed electron beam additively manufactured (*EBAM*) austenitic stainless steel *AISI 321* and to determine the optimal cutting parameters when machining on both industrial (including dry machining) and semi-industrial (universal, easily reconfigurable) *CNC*

machines, for which the corresponding recommendations from cutting tool manufacturers cannot always be directly applied.

The purpose of this study was to select the optimal values for the process parameters of finish milling (spindle speed, feed rate, and depth of cut / cutting width) based on a simultaneous evaluation of the machined surface roughness and material removal rate (*MRR*) during the machining of workpieces made of *EBAM AISI 321* austenitic stainless steel. To address the aim, the following ***objectives*** were set:

– assessment of mechanical properties of *EBAM AISI 321* stainless steel;

– establishing a correlation between cutting speed and feed rate and the cutting force during dry machining on a conventional (industrial) machine;

– establishing the relationship between the *MRR* and surface roughness and milling parameters during machining on a semi-industrial large-format *CNC* milling machine with coolant, employing both multiple linear regression models and non-linear models based on feedforward neural networks (*FFNN*).

Methods

AISI 321 steel wire with a diameter of 1.2 mm was used as the feedstock. In all cases, *AISI 321* steel plates, 5 mm thick, were used as substrates, which were initially ground and cleaned with acetone.

Samples were fabricated using an electron beam wire-feed additive manufacturing (*EBWAM*) facility with a vacuum chamber volume of 8 m³, developed by the Institute of Strength Physics and Materials Science *SB RAS* [17]. A thick wall with dimensions of 85 mm × 20 mm × 25 mm (Fig. 1) was built from the 1.2 mm diameter wire at an accelerating voltage of 30 kV, a chamber pressure of 5×10^{-3} Pa, a beam travel speed of 400 mm/min, and a wire feed rate of 1,768 mm/min. A circular beam oscillation pattern was applied with a beam diameter of 4 mm at a frequency of 1 kHz. The beam current was 75 mA for the first layer and 50 mA for all subsequent layers, with a layer height of 1 mm. The chemical composition of the wire is shown in Table 1.

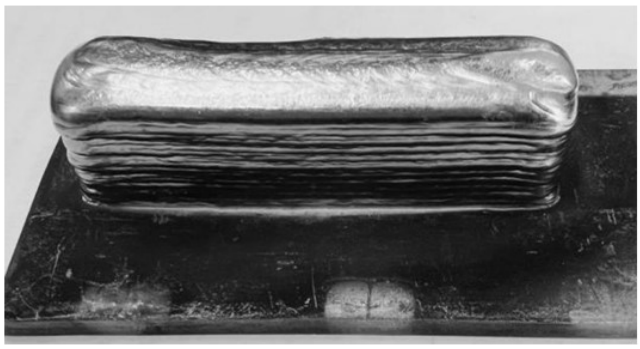

Fig. 1. Photographs of the 3D-built *EBAM 0.12C-18Cr-10Ni-Ti sample*

Table 1

Chemical composition of the *0.12C-18Cr-10Ni-Ti* stainless steel wire

Chemical composition, wt%								
Fe	*Cr*	*Ni*	*Mn*	*Ti*	*Si*	*Cu*	*Mo*	*Co*
65.3	19.6	11.5	0.8	0.7	0.7	0.5	0.32	0.7

Microhardness was measured using an automated system based on an *EMCO-TEST DuraScan-10* microhardness tester. Measurements were conducted according to the *Vickers* method under a load of 1 kgf with a dwell time of 10 seconds. Uniaxial tensile tests were performed on a *UTS-110M-100* electromechanical testing machine. The *crosshead* speed was 2 mm/min.

Milling of the additively manufactured blanks under dry conditions was performed on a *FU-251* (Russia) milling machine. The cutting force was measured using a *Kistler 9257B* (Switzerland) dynamometer (Fig. 2, *a*). Data analysis was conducted using *DynoWare* software. The dynamometer's resolution is 7.5 N, with a linearity error of ±0.005 %. Across multiple experimental runs (involving workpiece or tool repositioning) under identical parameters, the measured force variation did not exceed 15%. In machining processes, this represents acceptable repeatability, considering the complexity of the cutting process and potential inhomogeneity of the workpiece material.

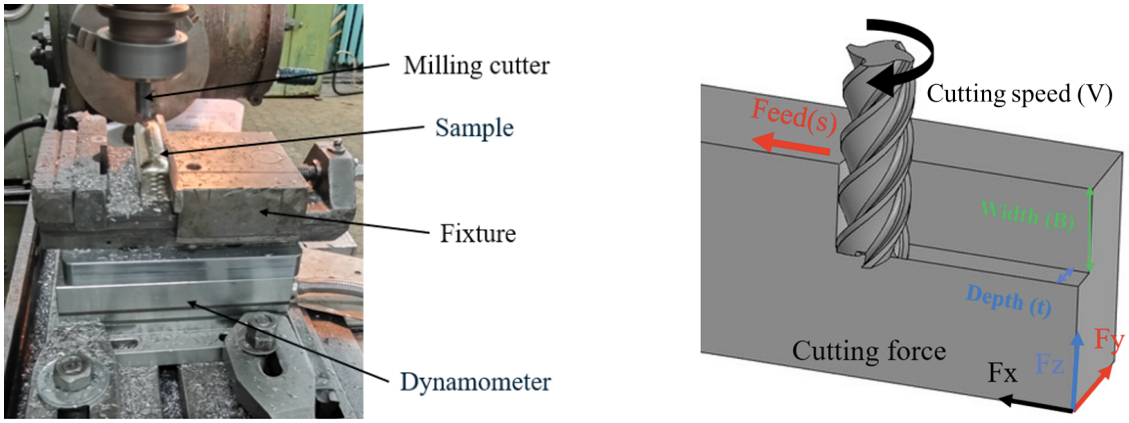

a *b*

Fig. 2. General view of the setup fixed on the milling machine (*a*); milling scheme (*b*)

Fig. 2, *b* shows the milling parameters, including feed per tooth (f_z), cutting speed (v_c), depth of cut (a_p), width of cut (***B***), and the resultant cutting force (***F***). Solid carbide end mills (*GESAC UP210-S4-12030*) with a diameter of 12 mm were used. The helix angle was **ω** = 35°, the flute length was 30 mm, the overall length was 75 mm, the rake angle (**γ**) was 7°, and the clearance angle (**α**) was 5°.

Research on milling workpieces made of *EBAM AISI 321* stainless steel with coolant was conducted on a large-format *PureLogic RM0813 CNC* milling machine (Russia) (Fig. 3, *a*). This machine is designed for milling, drilling, engraving, and cutting parts from non-ferrous metals and plastics, with the following specifications: spindle power of 2.2 kW, working volume (*X* × *Y* × *Z*) of 1,300 × 800 × 200 mm, and a positioning accuracy of 0.1 mm over 100 mm. Solid carbide end mills (***ZC-CCT VSM-4E-D8.0***) with a diameter of 8 mm were utilized. The variable helix angle was **ω** = 38°/41°, the flute length was 20 mm, the overall length was 60 mm, the rake angle (**γ**) was 7°, and the clearance angle (**α**) was 10°. The surface roughness (R_a) of the milled side faces of the workpieces was measured using a ***TR200*** (China) stylus profilometer (Fig. 3, *b*). To enhance productivity and reduce cutting force when using coolant, higher values of cutting speed and feed rate were employed.

The *Taguchi* method was used for designing the machining experiments. This method employs the signal-to-noise ratio (***S/N*** ratio) as an optimization criterion to evaluate the robustness and reliability of output parameters (primarily surface roughness) and utilizes orthogonal arrays to minimize the number of experimental runs [18, 19]. The Taguchi method is widely used to analyze the influence of various process parameters on output quality characteristics [20]. An L_9 orthogonal array was selected. The milling

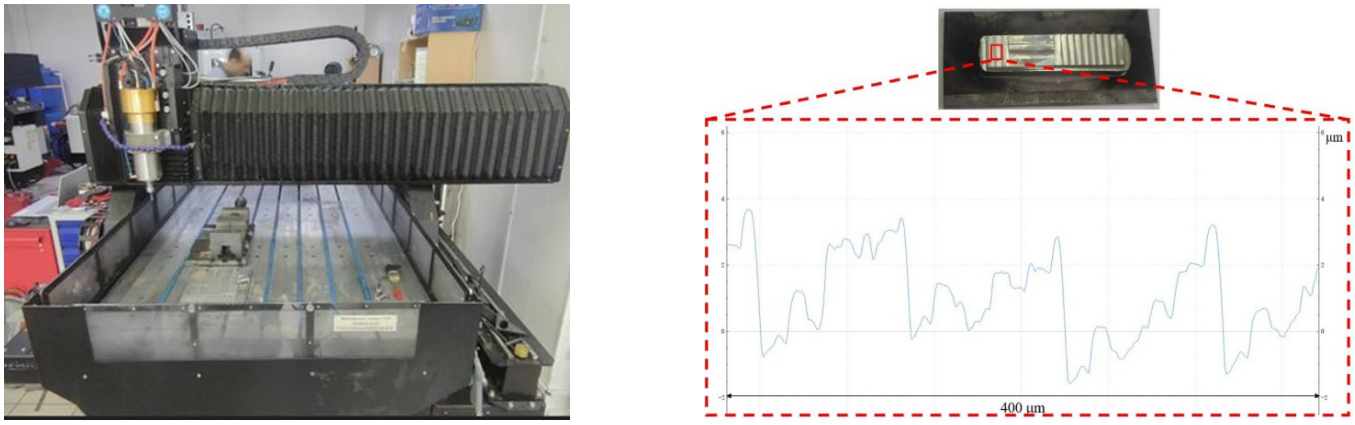

a *b*

Fig. 3. The *RM0813-01S2 CNC* machine (a); an example of the surface profile after milling (*b*)

process parameters (factors: spindle speed ***n***, feed rate ***S***, and width of cut ***B***) and their levels are presented in Table 2. Three levels were chosen for each factor, which also determine the material removal rate (*MRR*). The key output response was surface roughness (R_a).

Table 2

Mechanical properties of the *EBAM 0.12C-18Cr-10Ni-Ti* sample

Samples	Tensile strength, MPa	Yield strength, MPa	Elongation, %	Hardness, HV
EBAM 0.12C-18Cr-10Ni-Ti	570±10	208±10	70±2	191±5
Wrought 0.12C-18Cr-10Ni-Ti	700 ± 10	250 ± 10	63 ±3	230 ±5

Results and Discussion

The hardness and other key mechanical properties of the investigated samples are presented in Table 2. The *EBAM AISI 321* stainless steel exhibited high ductility (70 %), tensile strength (570 MPa), and hardness (191 HV). The strength properties of the wrought *AISI 321* steel were higher than those of the additively manufactured sample, which is attributed to the wrought condition, characterized by higher ferrite content, finer grain, and a higher dislocation density [21]. For the *EBAM* sample, the layer-by-layer deposition process involved multiple thermal cycles, leading to the formation of columnar grains. However, the corrosion rate of the wrought *AISI 321* steel was approximately twice as high as that of the additively manufactured steel.

Machinability Studies on a Stationary Milling Machine. As shown in Table 3, nine milling modes were used to investigate the variation in cutting force for the *EBAM AISI 321* stainless steel workpieces. These modes included combinations of low speed with high feed, high speed with low feed, and medium speed with medium feed.

The selection of milling parameters was based on the tool manufacturer's recommendations. It should be noted that using a high-performance milling regime (a high width-to-depth ratio, see Table 3) helps reduce rapid tool wear.

Fig. 4, *a* shows the influence of different milling regimes on the cutting force for the *EBAM AISI 321* stainless steel workpiece. The resultant cutting force (F_{xyz}), calculated as the vector sum, was used for evaluation according to Equation (1):

$$F_{xyz} = \sqrt{\left(F_X^{\max}\right)^2 + \left(F_Y^{\max}\right)^2 + \left(F_Z^{\max}\right)^2}, \quad (1)$$

where $F_{\max}$ is the maximum force value within the analysis interval.

Table 3

Parameters applied for studying the cutting forces during milling using the industrial machine

Number	Cutting speed **V**, m/min	Feed rate **S**, mm/min	Width **B**, mm	Depth **t**, mm
1	25	50	8	0,5
2	25	160		
3	25	250		
4	50	50		
5	50	160		
6	50	250		
7	75	50		
8	75	160		
9	75	250		

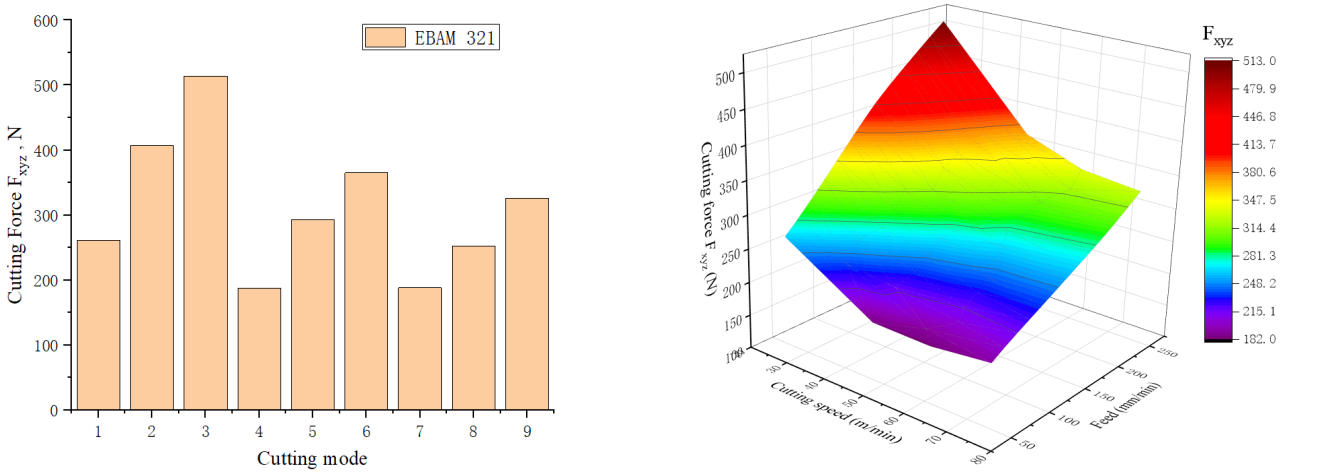

a *b*

Fig. 4. The effect of different cutting modes on the cutting force (*a*); the effect of cutting speed and feed rate on the cutting force during machining (*b*)

It was found that Mode No. 4 resulted in the smallest cutting force ($\boldsymbol{F_{xyz}}$ **= 188 N**).

Fig. 4, *b* shows the influence of cutting speed ($\boldsymbol{v_c}$) and feed per tooth ($\boldsymbol{f_z}$) on the cutting force during machining of the *EBAM* workpiece. It is evident that the strength and hardness of the additively manufactured steel significantly affected the cutting force. Low cutting speed combined with high feed rate led to an increase in cutting force, while high cutting speed with low feed rate reduced it.

Overall, two trends were observed: the cutting force decreased with increasing cutting speed and increased with increasing feed rate. When the depth ($\boldsymbol{a_p}$) and width ($\boldsymbol{B}$) of cut remain constant, a higher feed rate increases productivity. Therefore, to machine *EBAM AISI 321* steel with increased productivity and reduced cutting force, a higher cutting speed should be used, while the feed rate should not be increased excessively.

Machinability studies on the large-format *RM0813 CNC* milling machine. It is known that surface roughness depends on numerous parameters, including cutting speed, feed rate, depth of cut, and tool wear [22]. Table 4 shows the milling parameters used to investigate surface roughness ($\boldsymbol{R_a}$) and *MRR*, including spindle speed ($\boldsymbol{n}$), feed rate ($\boldsymbol{S}$), and width of cut ($\boldsymbol{B}$).

As noted earlier, machining on large-format *CNC* milling machines may be performed using regimes that differ from the cutting tool manufacturers' recommendations. Therefore, developing approaches to

Table 4

Milling parameters for the semi-industrial machine, determined using the *Taguchi* method and machinability assessment results

Number	Spindle speed *N*, rpm	Feed rate *S*, mm/min	Width *B*, mm	Depth *t*, mm	Surface roughness *Ra*, μm	*MRR*, mm³/min
1	1,000	200	0.1	4	0.46±0.02	80
2	1,000	400	0.3		1.29±0.04	480
3	1,000	600	0.5		2.57±0.23	1200
4	2,500	200	0.3		0.59±0.03	240
5	2,500	400	0.5		1.01±0.04	800
6	2,500	600	0.1		0.88±0.04	240
7	4,000	200	0.5		0.63±0.03	400
8	4,000	400	0.1		0.40±0.01	160
9	4,000	600	0.3		0.75±0.03	720

determine optimal milling parameters with minimal time and cost is highly relevant. Determining optimal cutting parameters can be considered a task of finding milling regimes that satisfy an optimality condition.

The optimality criterion should provide a comprehensive assessment of both the milling process efficiency and the finished product quality. Among the process characteristics, the material removal rate (*MRR*) was analyzed, while product quality was characterized by the post-processing surface roughness ($\boldsymbol{R_a}$). Tool wear, another critical characteristic, was excluded from these experiments as the selected regimes were conservative and the testing duration was short. Consequently, the optimality criterion can be formulated as a system of boundary expressions:

$$\begin{cases} Ra(S,B,N) \to \min, \\ MRR(S,B) \to \max. \end{cases} \quad (2)$$

Based on expression (2), a more formal suboptimality criterion can be derived as a system of inequalities:

$$\begin{cases} Ra(S,B,N) \le \overline{R_a}, \\ MRR(S,B) \ge \overline{MRR}. \end{cases} \quad (3)$$

where $\overline{R_a}$ and $\overline{MRR}$ are the maximum allowable roughness and minimum required *MRR*, respectively.

The range of parameters (***S***, ***B***, ***n***) satisfying the system of inequalities (3) defines the region of suboptimal parameters (*SOP*) [23].

The results of the acceptable milling parameters analysis are presented in Table 5. The used linear regression ("Regress") model had the following statistics: coefficient of determination $\boldsymbol{R^2} = 0.884$, normalized mean square error ***NMSE*** = 0.214, and significance level ***p*** = 0.0089. Based on this model, predicted roughness values were calculated within the allowable parameter range, the *SOP* satisfying condition (3) was identified, and a response surface graph for this region was plotted (Fig. 5, *a*, *c*). Despite the obtained high-quality metrics of the regression model, the hypothesis of a non-linear relationship between roughness and milling parameters was subsequently tested.

Based on the data from the L_9 *Taguchi* design experiments (see Table 4), the coefficients for the multiple linear regression were calculated using the least squares method [24–26]. The resulting roughness equation is:

$$R_a = 0.2014 - 0.00028N + 0.0021S + 2.059B. \quad (4)$$

As a non-linear modeling approach capable of generalizing experimental results, feedforward neural network (*FFNN*) modeling was chosen [27–28]. The network architecture was selected following the principle "from simple to complex". The training dataset was formed from experimental data (Table 4) with normalization of input and output values within the limits specified in Table 5. The best convergence

Table 5

Limiting ranges and suboptimality boundaries for the milling parameters and analyzed characteristics

	Permissible limits		Suboptimality boundaries	
	Min	Max	Min	Max
Parameter				
Spindle speed ***N***, rpm	500	5,000		
Feed rate ***S***, mm/min	100	800		
Width ***B***, mm	0.1	1		
Characteristics				
Surface roughness ***Ra***, μm	0	4	–	0.8
MRR, mm^3/min	0	2,000	300	–

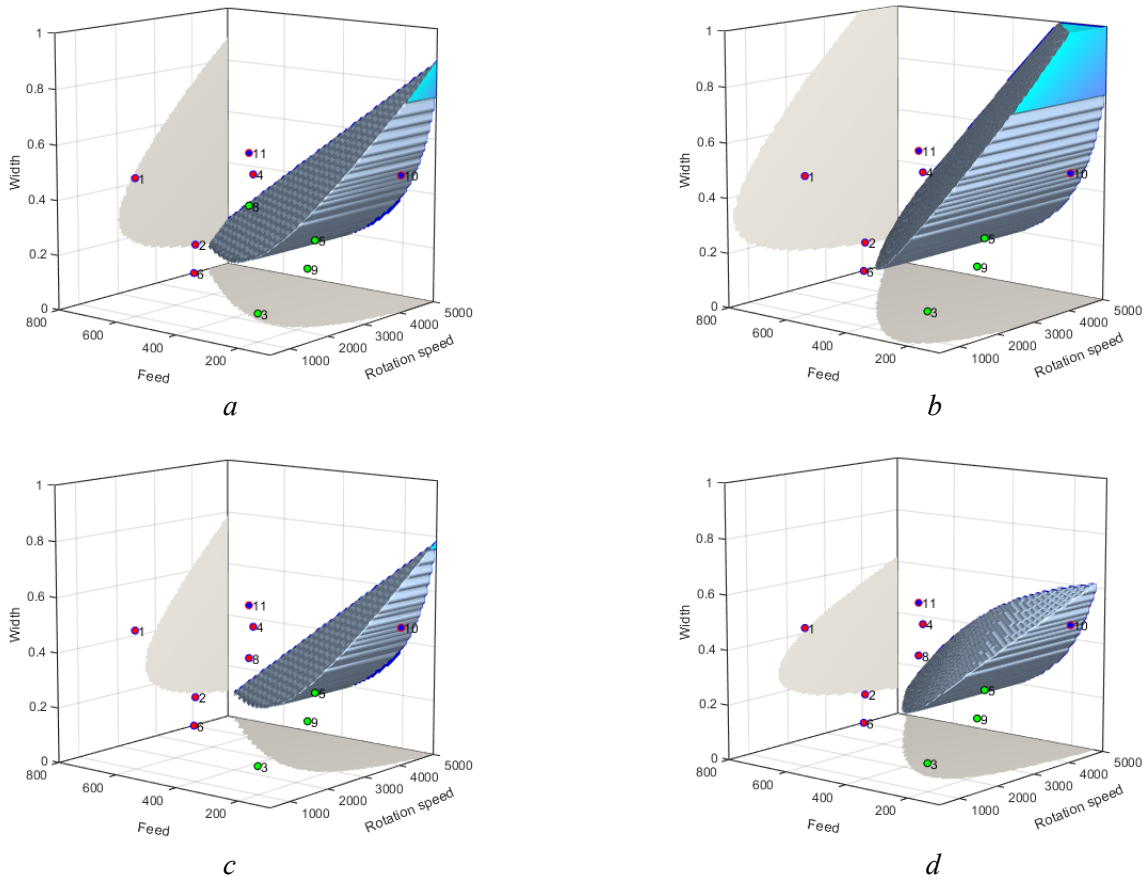

Fig. 5. Milling parameters and the *SOP* regions plotted using the linear regression model (*a, c*) and the *FFNN* model (*b, d*) at $\overline{p}$ = 300 mm^3/min; $\overline{Ra}$ = 0.8 μm (*a, b*) and $\overline{Ra}$ = 0.6 μm (*c, d*)

rate during training was achieved using the logarithmic tangent activation function and the *Levenberg-Marquardt* optimization algorithm. The number of layers and neurons per layer was chosen based on the analysis of the resulting model's *SOP*.

Among all considered variants, a network with one hidden layer containing three neurons was selected, as it demonstrated the simplest and most plausible *SOP* (Fig. 5, *b*, *d*). This model showed better agreement with the training dataset compared to the regression model: $\boldsymbol{MSE}$ = 0.00049061, $\boldsymbol{R^2}$ = 0.99504.

Comparing the obtained results, it was concluded that the *FFNN* model constrained the *SOP* region from above with a surface that was close to linear but had a steeper slope for high roughness values ($\overline{\boldsymbol{Ra}}$ > 0.65 μm). In other words, the *FFNN* model included milling parameters with higher width of cut and *MRR* values in the low-feed *SOP* region. For low roughness values ($\overline{\boldsymbol{Ra}}$ < 0.65 μm), this non-linear surface had the opposite effect: parameters with high width of cut and spindle speed were excluded from the *SOP*.

To verify the identified discrepancies, the developed models were validated through physical experiments by comparing predicted and actual surface roughness measurements. The experimental parameters were selected according to the following conditions: values outside the predicted *SOP* (No. 10, Table 6), boundary values of the *SOP* (No. 11, Table 6), and an internal point within the *SOP* (No. 12, Table 6). Table 6 also includes the predicted and experimental roughness values.

It was established that both models provided errors within an acceptable range, but the linear regression model demonstrated higher accuracy in terms of mean deviations. Its prediction for the optimal milling parameters is: spindle speed $\boldsymbol{n}$ = 4500 rpm, feed rate $\boldsymbol{S}$ = 404 mm/min, and width of cut $\boldsymbol{B}$ = 0.43 mm, with a predicted roughness $\boldsymbol{R_a}$ = 0.648 μm and a material removal rate *MRR* = 695 mm^3/min.

Holkar, H., et al. [29] selected optimal cutting parameters for milling *AISI 321* stainless steel using the Taguchi method. The study considered the effect of spindle speed, feed rate, and depth of cut on surface roughness, tool wear, and *MRR*. *Arlyapov, A.*, et al. [30] compared various tool geometries, cutting speeds,

Table 6

Milling parameters for model verification, along with experimental and predicted results

No.	Milling parameters			Characteristics			
	Spindle speed ***N***, rpm	Feed rate ***S***, mm/min	Width ***B***, mm	*MRR*, mm^3/min	Surface roughness ***Ra***, μm		
					Experiment	Regress	*FFNN*
10	4,000	100	0.5	200	0.333	0.3117	0.6115
11	4,000	600	0.5	1200	1.193	1.3617	1.0429
12	4,500	400	0.3	480	0.425	0.3889	0.5224
Average deviation						0.0753	0.1753

feed rates, and depth-to-width of cut ratios to evaluate tool wear and cutting force. It was shown that selecting milling parameters is a complex multi-criteria problem requiring extensive experimentation. A promising direction of the present research is the evaluation of factors affecting the surface roughness of *EBAM AISI 321* samples while ensuring a high *MRR*.

In summary, comparing the machinability assessment data for the industrial (dry) and the semi-industrial large-format *CNC* (with coolant) milling machines during finish milling of *EBAM AISI 321* stainless steel indicates that to achieve a higher *MRR*, reduced roughness, and lower cutting force, the cutting speed should be increased, while the feed rate should not be raised proportionally.

Furthermore, the developed regression and *FFNN* models for the semi-industrial machine enable the prediction of optimal process parameters, which is highly relevant for optimizing 3D-printing parameters that influence the microstructure and mechanical properties of layer-by-layer fabricated workpieces. Tool wear remains an important factor in assessing material machinability, as surface roughness increases with machining time due to cutting tool wear.

Future research plans include using the linear regression model to determine the optimal parameter range, followed by investigating the influence of machining time on tool wear and surface roughness.

Conclusion

1. Additively manufactured (*EBAM*) *AISI 321* stainless steel, fabricated with the utilized process parameters, exhibited high ductility (70 %), tensile strength (570 MPa), and hardness (191 HV).

2. It was established that to increase the material removal rate and reduce the cutting force during dry milling on a conventional milling machine, it is recommended to increase the cutting speed, while avoiding a proportional increase in the feed rate.

3. To investigate the relationship between material removal rate, surface roughness, and milling parameters on a semi-industrial large-format *CNC* milling machine (with a portal frame of moderate stiffness) under coolant supply, both multiple linear regression and non-linear feedforward neural network (*FFNN*) models were employed. It was shown that a linear regression model provided sufficient accuracy for predicting optimal milling parameters under the given conditions. However, the study was conducted within a narrow range of conservative regimes, with short machining times and without accounting for tool wear. Within these constraints, the following optimal milling parameters for the *EBAM AISI 321* were identified: spindle speed of 4,500 rpm, feed rate $\boldsymbol{S}$ = 404 mm/min, and width of cut $\boldsymbol{B}$ = 0.43 mm, yielding a predicted surface roughness of $\boldsymbol{R_a}$ = 0.648 μm and a material removal rate of 695 mm^3/min.

References

1. Lippold J.C., Kotecki D.J. *Welding metallurgy and weldability of stainless steels*. Hoboken, John Wiley & Sons, 2005. 357 p. ISBN 978-0-471-47379-4.

2. Huang Z., Zhang J., Ma Z., Yuan S., Yang H. Research progress on the relationship between microstructure and properties of AISI 321 stainless steel. *Applied Sciences*, 2024, vol. 14 (22), p. 10196. DOI: 10.3390/app142210196.

3. Yin Q., Chen G., Cao H., Zhang G., Zhang B., Wei S. Transformation law of microstructure evolution and mechanical properties of electron beam freeform fabricated 321 austenitic stainless steel. *Vacuum*, 2021, vol. 194, p. 110594. DOI: 10.1016/j.vacuum.2021.110594.

4. Ma M., Wang Z., Gao M., Zeng X. Layer thickness dependence of performance in high-power selective laser melting of 1Cr18Ni9Ti stainless steel. *Journal of Materials Processing Technology*, 2014, vol. 215, pp. 142–150. DOI: 10.1016/j.jmatprotec.2014.07.034.

5. Kameneva A.L., Minkova A.A., Cherkashneva N.N., Karmanov V.V. Correlation between heat treatment process parameters, phase composition, texture, and mechanical properties of 12H18N10T stainless steel processed by selective laser melting. *IOP Conference Series: Materials Science and Engineering*, 2018, vol. 447 (1), p. 012043. DOI: 10.1088/1757-899X/447/1/012043.

6. Wang X., Hu Q., Liu W., Yuan W., Shen X., Gao F., Tang D., Hu Z. Microstructure and corrosion properties of wire arc additively manufactured multi-trace and multilayer stainless steel 321. *Metals*, 2022, vol. 12, p. 1039. DOI: 10.3390/met12061039.

7. Zhong C., Gasser A., Backes G., Fu J., Schleifenbaum J.H. Laser additive manufacturing of Inconel 718 at increased deposition rates. *Materials Science and Engineering: A*, 2022, vol. 844, p. 143196. DOI: 10.1016/j.msea.2022.143196.

8. Sciaky Inc. *Benefits of Wire vs. Powder Metal 3D Printing. Comparing Sciaky's wirefeed 3D printing process, a.k.a. Electron Beam Additive Manufacturing, to powder-based feedstock 3D printing processes*. Available at: https://www.sciaky.com/additive-manufacturing/wire-vs-powder (accessed 30.10.2025).

9. Chen Y., Chen X., Jiang M., Lei Z., Wang Z., Liang J., Wu S., Ma S., Jiang N., Chen Y. Coaxial laser metal wire deposition of Ti6Al4V alloy: process, microstructure and mechanical properties. *Journal of Materials Research and Technology*, 2022, vol. 20, pp. 2578–2590. DOI: 10.1016/j.jmrt.2022.08.068.

10. Caballero A., Ding J., Ganguly S., Williams S. Wire + arc additive manufacture of 17-4 PH stainless steel: Effect of different processing conditions on microstructure, hardness, and tensile strength. *Journal of Materials Processing Technology*, 2019, vol. 268, pp. 54–62. DOI: 10.1016/j.jmatprotec.2019.01.007.

11. Węglowski M.S., Błacha S., Phillips A. Electron beam welding – Techniques and trends – Review. *Vacuum*, 2016, vol. 130, pp. 72–92. DOI: 10.1016/j.vacuum.2016.05.004.

12. Wang D., Liu Z., Liu W. Experimental measurement of vacuum evaporation of aluminum in Ti-Al, V-Al, Ti6Al4V alloys by electron beam. *Metals*, 2021, vol. 11 (11), p. 1688. DOI: 10.3390/met11111688.

13. Lyu Z., Sato Y.S., Tokita S., Zhao Y., Jia J., Wu A. Microstructural evolution in a thin wall of 2Cr13 martensitic stainless steel during wire arc additive manufacturing. *Materials Characterization*, 2021, vol. 182, p. 111520. DOI: 10.1016/j.matchar.2021.111520.

14. Martyushev N.V., Kozlov V.N., Qi M., Tynchenko V.S., Kononenko R.V., Konyukhov V.Yu., Valuev D.V. Production of workpieces from martensitic stainless steel using electron-beam surfacing and investigation of cutting forces when milling workpieces. *Materials*, 2023, vol. 16, p. 4529. DOI: 10.3390/ma16134529.

15. Ravi G.A., Hao X., Wain N., Wu X., Attallah M.M. Direct laser fabrication of three dimensional components using SC420 stainless steel. *Materials & Design*, 2013, vol. 47, pp. 731–736. DOI: 10.1016/j.matdes.2012.12.062.

16. Grzesik W. Hybrid additive and subtractive manufacturing processes and systems: A review. *Journal of Machine Engineering*, 2018, vol. 18, pp. 5–24. DOI: 10.5604/01.3001.0012.7629.

17. Klimenov V.A., Kolubaev E.A., Han Z., Chumaevskii A.V., Klopotov A.A., Ustinov A.M., Kovalevskaya Z.G, Moskvichev E., Pan M. Influence of anisotropy properties and structural inhomogeneity on elasticity and fracture of titanium alloys produced by electron-beam melting. *The International Journal of Advanced Manufacturing Technology*, 2024, vol. 135, pp. 5575–5594. DOI: 10.1007/s00170-024-14843-7.

18. Park S.H. *Robust design and analysis for quality engineering*. London, Chapman & Hall, 1996. 256 p.

19. Phadke M.S. *Quality engineering using robust design*. Englewood Cliffs, NJ, Prentice-Hall, 1989. 320 p.

20. Nalbant M., Gökkaya H., Sur G. Application of Taguchi method in the optimization of cutting parameters for surface roughness in turning. *Materials & Design*, 2007, vol. 28 (4), pp. 1379–1385. DOI: 10.1016/j.matdes.2006.01.008.

21. Panin S.V., Qi M., Stepanov D.Y., Burkov M.V., Rubtsov V.E., Kushnarev Y.V., Litovchenko I.Yu. Comprehensive analysis of microstructure and mechanical, operational, and technological properties of AISI 321 austenitic stainless steel at electron beam freeform fabrication. *Construction Materials*, 2025, vol. 5 (3), p. 62. DOI: 10.3390/constrmater5030062.

22. Zhang J.Z., Chen J.C., Kirby E.D. Surface roughness optimization in an end-milling operation using the Taguchi design method. *Journal of Materials Processing Technology*, 2007, vol. 184 (1–3), pp. 233–239. DOI: 10.1016/j.jmatprotec.2006.11.029.

23. Stepanov D.Y., Tian D., Alexenko V.O., Panin S.V., Buslovich D.G. Application of neural network models with ultra-small samples to optimize the ultrasonic consolidation parameters for 'PEI Adherend/Prepreg (CF-PEI Fabric)/PEI Adherend' lap joints. *Polymers*, 2024, vol. 16, p. 451. DOI: 10.3390/polym16040451.

24. Draper N.R., Harry S. *Applied regression analysis*. 3rd ed. Wiley-Interscience, 1998. 736 p. ISBN 0471170828. ISBN 9780471170822.

25. Kuprienko N.V., Ponomareva O.A., Tikhonov D.V. *Statisticheskie metody izucheniya svyazei: Korrelyatsionno-regressionnyi analiz* [Statistical methods for studying relationships]. St. Petersburg, SPbPU Publ., 2009. 118 p.

26. Yan X., Su X. *Linear regression analysis: Theory and computing*. Singapore, World Scientific Publishing, 2009. 328 p. ISBN 9812834109. ISBN 9789812834102.

27. Haykin S.S. *Neural networks and learning machines*. 3rd ed. Upper Saddle River, NJ, Pearson Education, 2009. ISBN 978-0131471399.

28. Swingler K. *Applying neural networks: A practical guide*. San Francisco, CA, Morgan Kaufman Publishers, 1996. 303 p. ISBN 0126791708. ISBN 9780126791709.

29. Holkar H., Sadaiah M. Optimization of end milling machining parameters of AISI 321stainless steel using Taguchi method. *International Journal on Recent and Innovation Trends in Computing and Communication*, 2016, vol. 4, pp. 20–23.

30. Arlyapov A., Volkov S., Promakhov V., Matveev A., Babaev A., Vorozhtsov A., Zhukov A. Study of the machinability of an Inconel 625 composite with added NiTi-TiB_2 fabricated by direct laser deposition. *Metals*, 2022, vol. 12 (11), p. 1956. DOI: 10.3390/met12111956.

Conflicts of Interest

The authors declare no conflict of interest.